Large eddy simulation for the rapid phase transition of LNG

15 August 2024

Large Eddy Simulation for the Rapid Phase Transition of LNG

Abstract

The environmental concerns on the use of fossil fuels have incentivized the utilization of cleaner solutions for energy supply. Natural gas in the form of a liquid (LNG) is considered a promising and highly attractive alternative due to the high density and relatively low cost of transportation.

In the case of accidental release on water, elevated heat transfer causes rapid evaporation that has the potential to lead to a rapid phase transition (RPT), thus producing significant overpressures.

In this work, the effects of composition, release rate, and the fluid dynamic regime of water on the RPT of LNG are analyzed by means of detailed analysis based on computational fluid dynamics and large eddy simulation for the turbulence model. The thermodynamic properties at ultra-low temperature related to the species considered in the mixtures are estimated by using an approach based on quantum mechanics.

Results are compared with experimental analysis, quite satisfactorily. A preliminary conclusion shows that calm water, as within port facilities, decreases the likelihood of the RPT or its magnitude to a negligible intensity. On the contrary, the addition of ethane or propane may dramatically affect the explosive phenomenon.

1. Introduction

The last decades have been characterized by the continuous increase of attention toward the environments, promoting the development of alternative solutions for energy production. Among them, natural gas has been indicated as promising fuel [1]. The existence of significant reservoirs located in remote areas has actively encouraged the liquefaction processes because of the increased density and reduced capital cost for the compressed gas [2]. However, the implementation of LNG on large scales has arisen serious concerns related to the accuracy of existing models adopted for safety evaluations [3], or to the applicability and robustness of existing procedures developed for more traditional conditions [4]. Indeed, ultra-low temperature conditions are accompanied by poor understanding of several physic-chemical models (e.g., evaporation rate [5], dense gas dispersion and stratification [6], and combustion [7]), interactions with traditional mitigation systems [8][9], and the likelihood of unconventional accidental scenarios [10]. Besides, the effects of LNG composition on consequence analysis is still poorly understood for several accidental scenarios [11]. Regardless of the presence of ignition sources in the proximity of the releasing point, in the case of accidental release of LNG on water, the intimate mixing between two liquids and the difference between bubble point of the mixture and room temperature may lead to extremely elevated evaporation rates, thenceforth referred to as rapid phase transition (RPT), potentially causing significant shock waves [12] and vapour cloud explosions [13]. Several examples of industrial accidents and large scale tests have been reported in the literature [14][15]. Quite obviously, these scenarios spawn concerns especially in shore installations, where elevated congested areas can be present, posing the attention on risk related to bunkering procedures [15]. Hence, safety parameters should represent a pillar in policy generation to secure long-term operation and business development [16].

In this light, the utilization of theoretical-sound models for the prediction of the evaporation rate is essential for meaningful estimations of RPT related scenarios [17]. To this aim, several models can be adopted [18][19][20]. However, most of them are empirical-based, developed, and validated in non-cryogenic conditions. Hence, their applicability for the evaluation of the accidental release of LNG should be carefully evaluated with preliminary investigations. Besides, different boiling regimes (e.g., nucleate boiling, transition regime, and film boiling) can be distinguished [21][22] and significantly affect the overall heat transfer coefficients. This phenomenon makes crucial the prediction of the transition temperatures and the corresponding maximum and minimum heat fluxes [23]. This is particularly true for the condition leading to the change from transition to nucleate boiling, often referred to as Leidenfrost temperature (or point) [24]. Indeed, the Leidenfrost point is mainly affected by the composition of the boiling liquid and, together with superheat limit temperature, can be used as a trigger criterion for RPT [10]. The former can be estimated by using the correlation developed by Kalinin and co-workers [25], whereas several data related to the latter parameter has been reported by Reid [26] during his pioneering studies on the subject. Considering the difference between LNG and water temperatures, the film boiling regime is often assumed. Under this hypothesis, a theoretical based model developed by Klimenko [27] has been implemented for the LNG case [5], resulting in evaporation rate of 0.07 kg m^{-2} s^{-1}. This value is in line with the lower bound of the experimental measurements reported in a dedicated literature review [28]. Moreover, Parihar et al. [29] suggest that the evaporation from the LNG pool can be simulated by the injection of natural gas vapor with an evaporation rate of 0.135 kg m^{-2} s^{-1}. However, higher values, up to 0.20 kg m^{-2} s^{-1} have been reported [30]. This variability can be partially attributed to the turbulence of water [18], often not included in the experimental campaign reports, and promotes the evaluation of consequences for a larger evaporation rate, as well. Quite clearly, the initial LNG composition plays a significant role in the time evolution of the investigated scenario because of the different volatility

of the species forming the mixture, resulting in time-dependent liquid and vapor compositions. Besides, trustworthy estimations of thermodynamic properties at low-temperature conditions of each species involved are essential to guarantee accurate values. In this sense, the adoption of a theoretical approach, such as quantum mechanics calculations, is suggested to break away from the errors related to the non-ideal behaviour of the system [31].

Once the evaporation occurred, either the generated overpressure or the fuel concentration distributions for time and position are of interest for the sake of consequence analysis. The former generates blast waves commonly modeled assuming the acoustic approximation [12]. Although a localized impact characterizes them, blast waves are potentially able to damage storage systems in the surrounding area, triggering second cascading events [32].

Under this framework, in this work, the effects of LNG composition and release rate on RPT have been studied numerically, by selecting an appropriate theoretical approach for the calculation of thermodynamic properties theoretically.

2. Methodology

The present study was conducted using the computational fluid dynamic code OpenFOAM and the large eddy simulation (LES) approach for the analysis of turbulent flows [33]. For the sake of simplicity, a 2-dimensional domain was considered. The conservation equations of mass, momentum, species, and energy can be expressed as follow:

$$\frac{\partial \rho}{\partial t} + \frac{\partial \rho u_j}{\partial x_j} = S_{\delta,eva} + S_{p,eva} \tag{1}$$

$$\frac{\partial \rho u_j}{\partial t} + \frac{\partial \rho u_i u_j}{\partial x_j} = -\frac{\partial p}{\partial x_i} - g_i x_i \frac{\partial \rho}{\partial x_i} + \frac{\partial}{\partial x_j}\left[\tau_{ij} + \tau_{t,ij}\right] \tag{2}$$

$$\frac{\partial \rho Y_k}{\partial t} + \frac{\partial \rho u_j Y_k}{\partial x_j} = \frac{\partial}{\partial x_j}\left(\mu_{eff} \frac{\partial Y_k}{\partial x_j}\right) + R_k + S_{Yk,\delta} + S_{Yk,p} \tag{3}$$

where $S_{\delta,eva}$ is the source term of the liquid film evaporation, $S_{p,eva}$ is the source term of the liquid droplets, p is the gaseous pressure, τ_{ij} and $\tau_{t,ij}$ are the viscous and turbulent stress tensors, respectively, Y_k the mass fractions of the kth element, μ_{eff} the effective dynamic viscosity and R_k the velocity of every single reaction. Furthermore, the energy equation is expressed as a function of the enthalpy h:

$$\frac{\partial \rho h}{\partial t} + \frac{\partial \rho u_j h}{\partial x_j} + \frac{\partial \rho K}{\partial t} + \frac{\partial \rho u_j K}{\partial x_j} = \frac{\partial(q_i + q_{ti})}{\partial x_i} + \rho h_s + R_{ad} + \frac{\partial p}{\partial t} - \rho g_j u_j + \frac{\partial \tau_{ij} u_i}{\partial x_j} + S_{h\delta,eva} + S_{hp,eva} \tag{4}$$

$$h = e + \frac{p}{\rho} \tag{5}$$

$$k = \frac{1}{2} u_i u_j \tag{6}$$

where e is the internal energy, ρ the density, q_i the diffusive heat flux, q_{ti} the turbulent heat flux, h_s the heat source, R_{ad} the radiative heat, $S_{h\delta,eva}$ is the enthalpy source term of the evaporated mass from the liquid film and $S_{hp,eva}$ is the enthalpy source term of the evaporated mass from the particles.
For the aims of RPT analysis, particular attention was posed to the liquid spill (in the absence of ignition). Considering the different characteristic scales of the investigated phenomena, the

abovementioned system was divided into two sub-systems dividing the two phases, following the widespread numerical approach commonly adopted for heterogeneous systems [34]. Hence, a domain containing only the cryogenic liquid was defined for the estimation of the evaporation rate and vapor composition leaving the pool. Then, these results were considered as boundary conditions for the second sub-system, containing vapor and air. The pool was assumed of a circular shape. The inlet velocity was referred to as in the gas phase directly, as suggested by Halin-Luketa et al. [35] and, from now on, it will be indicated as the release rate v_r The corresponding evaporation rate (E_{vap}) expressed in mass per unit surface can be easily calculated by using the vapor density ρ_g at the liquid temperature:

$$E_{vap} = v_r \rho_g \tag{7}$$

The boundary conditions adopted in this work are reported in the following table.

Table 1. Summary of the boundary conditions adopted for the evaluation of LNG spills.

Parameter	
Initial LNG temperature	108 K
Room temperature	293.15 K
Pool diameter (inlet size), D	0.1 – 3.0 m
Domain sizes (L x H)	(4 x 12) m^2

The domain sizes were conveniently selected to reduce the effect of their boundaries on the obtained results for the case of a pool diameter of 1 m. To this aim, a structured grid having the cell sizes reported in Table 3 was adopted for the grid sensitivity analysis.

Table 2. Summary of the cell sizes adopted for the grid sensitivity analysis. Note that the x and y axes represent horizontal and vertical directions, respectively.

Mesh Name	Size on x [m]	Size on y [m]
Mesh 1	$10.0 \cdot 10^{-2}$	$10.0 \cdot 10^{-2}$
Mesh 2	$2.6 \cdot 10^{-2}$	$3.0 \cdot 10^{-2}$
Mesh 3	$1.0 \cdot 10^{-2}$	$1.3 \cdot 10^{-2}$
Mesh 4	$8.0 \cdot 10^{-3}$	$10.0 \cdot 10^{-3}$

The effect of the pool dimension was evaluated at first, by assuming a cylindrical pool characterized by a constant diameter. This parameter relies on the amount of LNG spilled and may significantly variate with the time after release during the early stages. Typically, diameters of about 30 m can be expected for uniquely large scale releases (e.g., the immediate release of 40 m^3 of LNG) [36]. On the other hand, smaller releases, e.g., caused by rupture of loading arms during the bunkering procedures, represent more credible scenarios for LNG operations [37]. In these cases, the quantities involved are significantly lower. The total arm length (intended as the sum of the length of the in/outboard arms) varies from 8.5 to 30 m, with a constant diameter of 0.30 m [38]. Hence, the release volume of LNG ranges from 0.6 to 2 m^3. In this light, pool diameter was variated between 0.1 – 3.0 m, to evaluate the different released amount and stages observable during the pool formation at the early stage that

follows the release. Afterward, a constant diameter of the pool equal to 1.0 m was considered for the following analyses.

In addition, the release rate v_r was gradually increased, starting from the lower values reported in the literature, associated with an accidental release on calm water conditions [5], until the minimum value causing structural damages. More specifically, it was increased from the initial value of 0.12 m s^{-1} up to 40 m s^{-1}. The effect of the LNG composition was also considered (Table 4). Light alkanes (i.e., methane, ethane, and propane) are distinguished by non-hydrocarbon species (e.g., nitrogen and carbon dioxide and traces of heavier compounds commonly present in natural gas), which have been conveniently merged and referred as "Inert" [39]. Three different compositions were assessed: pure methane (Mixture 1), representing the benchmark case; the heavier composition that should be referred to as natural gas (Mixture 3); and an intermediate composition (Mixture 2).

Table 3. Summary of the cell sizes adopted for the grid sensitivity analysis. Note that the x and y axes represent horizontal and vertical directions, respectively.

Mixture	CH$_4$ [w/w]	C$_2$H$_6$ [w/w]	C$_3$H$_8$ [w/w]	Inert [w/w]	ρ_g [kg m^{-3}]
Mix 1	100	0	0	0	1.79
Mix 2	84	10	4	2	1.82
Mix 3	70	18	8	4	1.83

A base case scenario having pool diameter equal to 1 m, composed of Mix 1, and evaporation rate equal to 0.21 kg m^{-2} s^{-1}, was defined for preliminary evaluations.

The thermodynamic properties related to the species considered in these mixtures and air were estimated by using an approach based on quantum mechanics. More specifically, optimized geometries, harmonic frequencies, and rotor scans (if hindered rotors are contained in the analyzed species) were calculated by using the CBS-QB3 level of theory [40]. To this aim, the rigid rotor harmonic oscillator (RRHO) approximation corrected for 1D hindered rotors was utilized, and the full rotation was divided into 45 sections of 8° each. Stable geometries were found for any configurations. The collected data were implemented in Automated Reaction Kinetics and Network Exploration (Arkane) tool [41] for the calculation of thermodynamic parameters. The whole procedure, including possible troubleshoot, was automated using an automated rate calculator (ARC) package [42].

3. Results and discussion

The collected data on thermodynamic properties were expressed in terms of NASA polynomial coefficients, to include the effect of temperature (Table 4). For the sake of simplicity, only the coefficients referring to the low-temperature range were reported, being all the intermediate temperature adopted in this work higher than 350 K, i.e., considerably higher than the maximum expected temperature in the case of absence of ignition. Oxygen and nitrogen coefficients were included for completeness.

Table 4. Low -temperature coefficients of NASA polynomial, as calculated for the species involved in this work.

Species	A_0	A_1	A_2	A_3	A_4	A_5	A_6
CH$_4$	$4.21 \cdot 10^0$	$-5.36 \cdot 10^{-3}$	$2.51 \cdot 10^{-5}$	$-2.14 \cdot 10^{-8}$	$5.97 \cdot 10^{-12}$	$-1.02 \cdot 10^4$	$-9.21 \cdot 10^{-1}$
C$_2$H$_6$	$3.75 \cdot 10^0$	$4.55 \cdot 10^{-5}$	$4.08 \cdot 10^{-5}$	$-4.57 \cdot 10^{-8}$	$1.57 \cdot 10^{-11}$	$-1.15 \cdot 10^4$	$4.74 \cdot 10^0$
C$_3$H$_8$	$3.06 \cdot 10^0$	$1.29 \cdot 10^{-2}$	$3.47 \cdot 10^{-5}$	$-4.71 \cdot 10^{-8}$	$1.71 \cdot 10^{-11}$	$-1.44 \cdot 10^4$	$1.08 \cdot 10^1$
N$_2$	$3.54 \cdot 10^0$	$-6.93 \cdot 10^{-4}$	$2.10 \cdot 10^{-6}$	$-1.29 \cdot 10^{-9}$	$2.59 \cdot 10^{-13}$	$-1.04 \cdot 10^3$	$2.99 \cdot 10^0$
O$_2$	$3.12 \cdot 10^0$	$1.73 \cdot 10^{-3}$	$-8.53 \cdot 10^{-7}$	$1.70 \cdot 10^{-10}$	$-1.23 \cdot 10^{-14}$	$-1.04 \cdot 10^3$	$6.28 \cdot 10^0$

These values were considered for the estimation of the main thermodynamic properties throughout the following investigations.

The base case scenario described in the previous section was analyzed for the individuation of optimized computational domains. It was evaluated by implementing different mesh sizes, and the results of this analysis were reported in terms of temperature distributions calculated along the vertical axis at the symmetry (Figure 1).
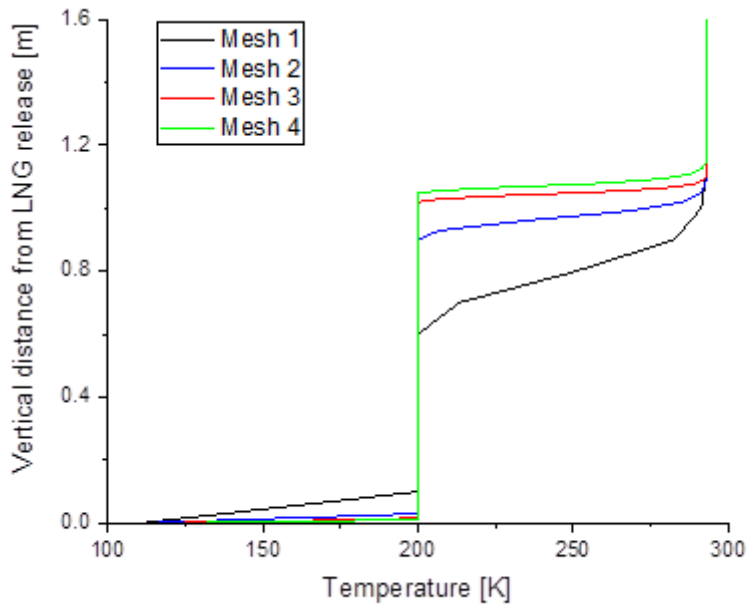

Figure 1 Numerical estimations of temperature distributions to the vertical distance from the release obtained with different meshes.

Considering the reported results, Mesh 4 was used to investigate the effect of the release rate v_r and mixture composition on the overpressure produced. Subsequently, the temporal and spatial evolution of the volume fraction of methane, for different v_r values were analyzed for the base case conditions (i.e., fixed mixture composition equivalent to Mix 1 and pool diameter equal to 1 m). More specifically, v_r of 10 m s^{-1} (Figure 2.a), 20 m s^{-1} (Figure 2.b), and 40 m s^{-1} (Figure 2.c) were assumed, respectively.
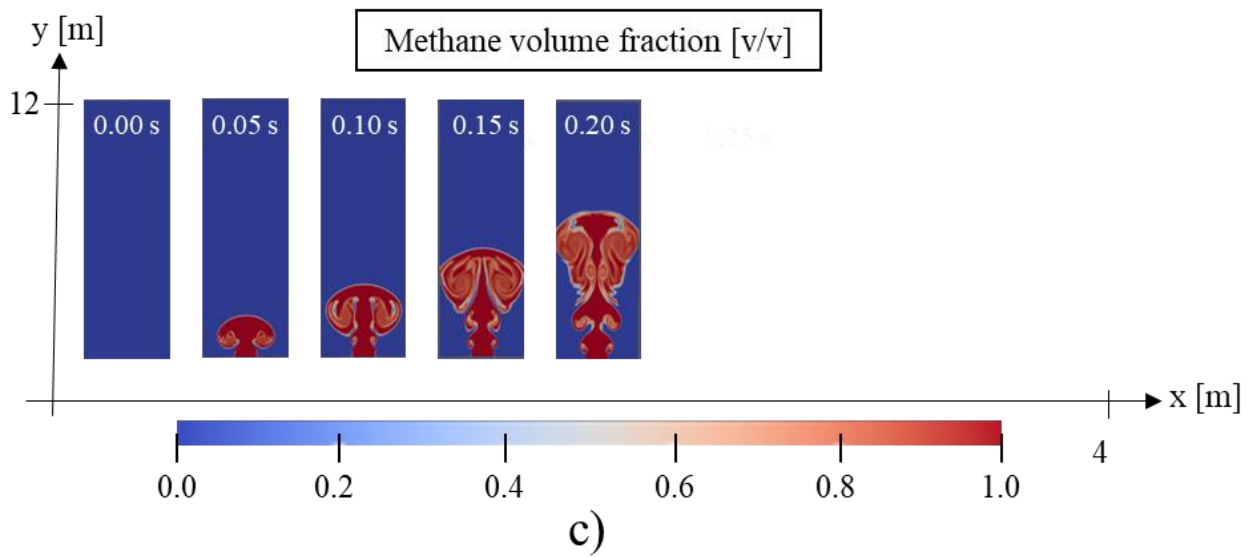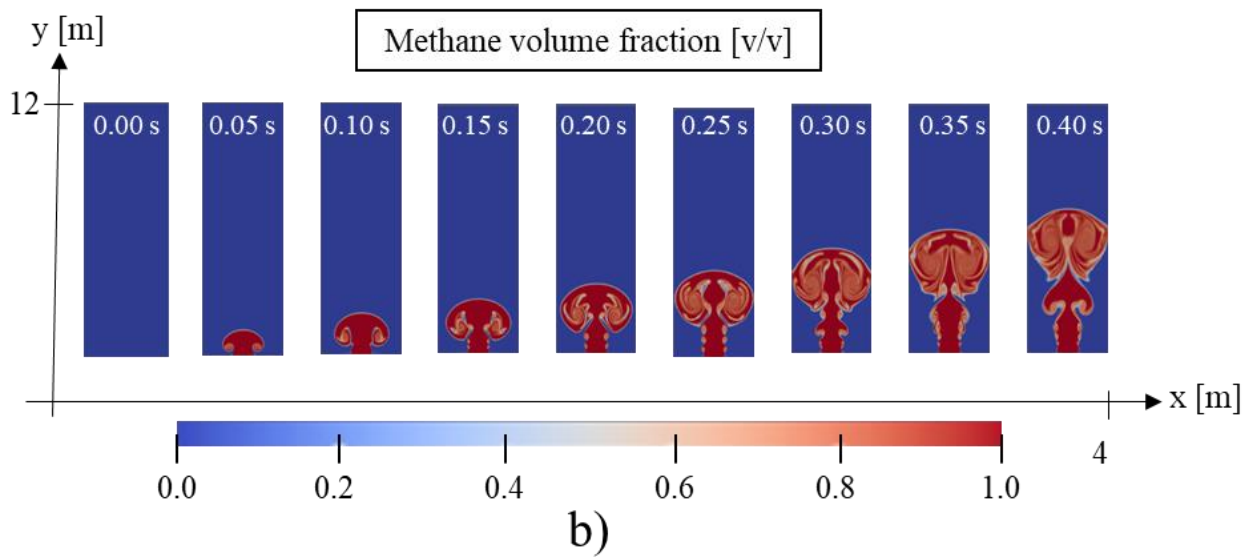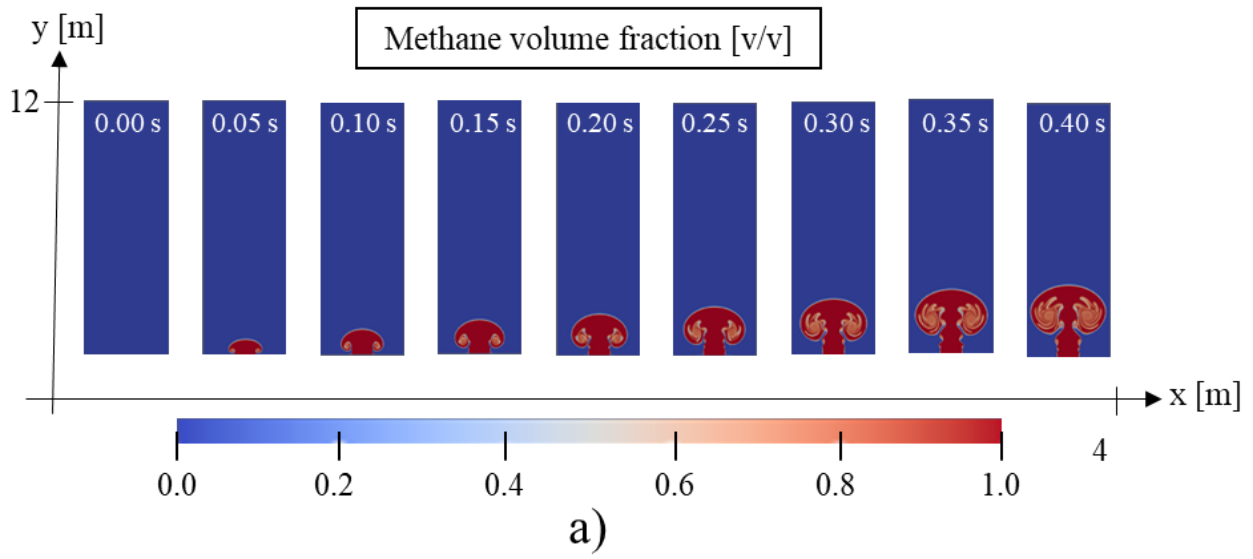
Figure 2 Time and spatial distribution of methane mole fraction with the release rate of 10 m s⁻¹ (a), 20 m s⁻¹ (b), and 40 m s⁻¹ (c), in case of mixture composition equal to Mix 1 (pure methane).

It is possible to observe that the differences in the release rate lead to an increase in the instability of the flow field. This increases the vorticity phenomena, especially on the side of the domain, and results in a more corrugated profile. Quite clearly, the higher the release rate, the greater the height reached (e.g., at 0.20 s, 2.0 m, 3.4 m, and 6.8 m, respectively). In addition to that, it is possible to affirm that the longer is the time, the higher is the mixing with the air. Simulations with 40 m s^{-1} (Figure 2.c) were stopped at 0.20 s due to elevated computational cost.

Typical overpressure curves for the three compositions analyzed in this work, as obtained by the CFD-LES simulations, are reported in Figure 3. For the sake of comparison, the dimensionless overpressure $\psi = (\Delta P / \Delta P_{max})$, assuming ΔP_{max} as the maximum overpressure observed for each time, with respect to the shifted time $\tau = (t - t_0)$ is reported, where t_0 represents the time where LNG came into contact with water.
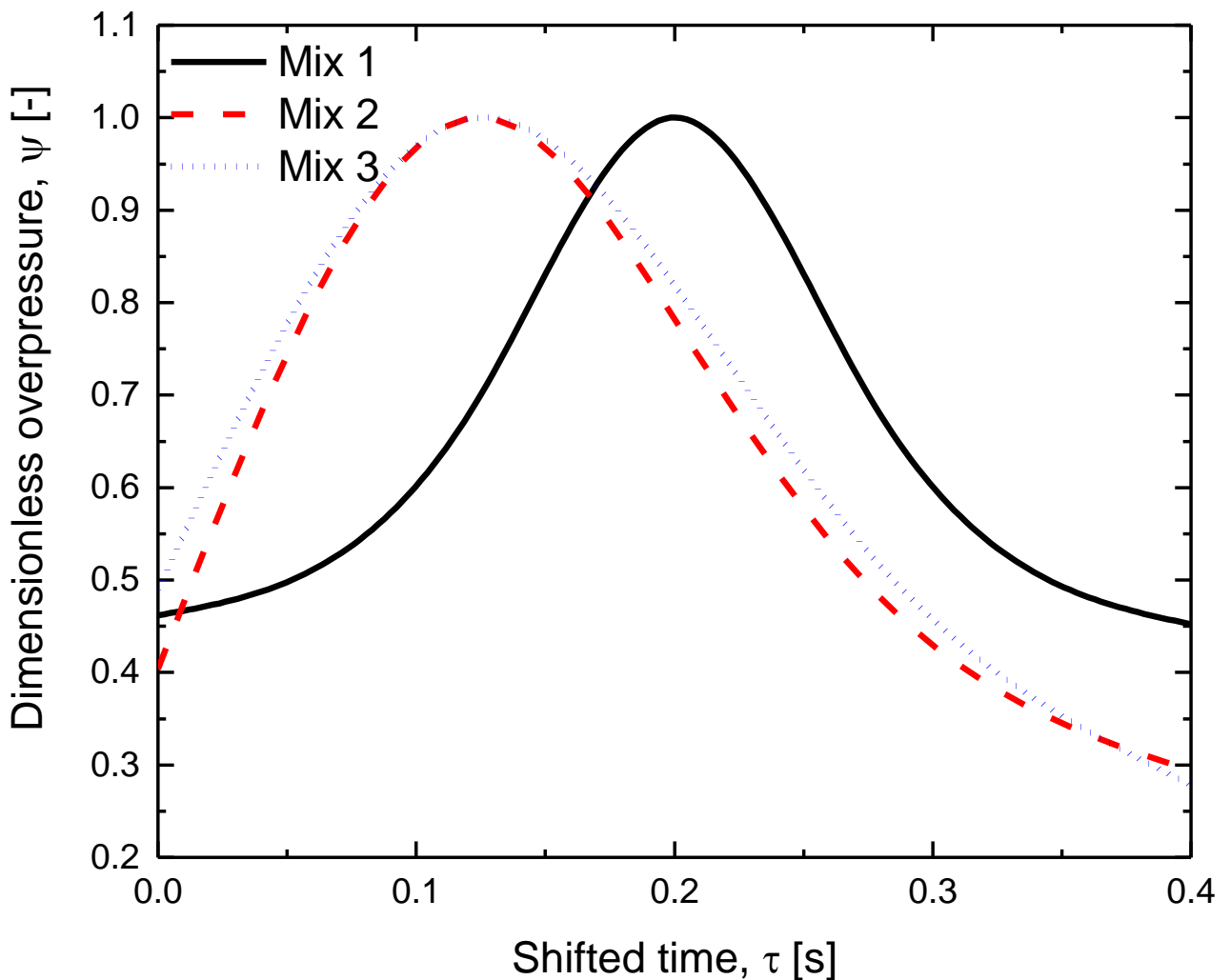

Figure 3. Dimensionless overpressure ($\Delta P / \Delta P_{max}$) as a function of the shifted time τ for different LNG compositions. The curves are chosen at the distance where the maximum overpressure was obtained at any time.

A typical bell-shape is observed for all the investigated mixtures. It is worth mentioning that variations between Mix 2 and Mix 3 are much lower than Mix 1. Indeed, the presence of ethane and

propane in the gaseous mixture significantly anticipates the overpressure peak concerning pure methane.

The evaluation of ΔP_{max} with respect to the boundary conditions may define the investigated scenario uniquely. The effect of pool diameter on ΔP_{max} was evaluated at first (Table 5). For the sake of conciseness, data related to Mix 1 (i.e., pure methane) were reported exclusively.

Table 5. Maximum overpressure (ΔP_{max}) generated by the release of pure methane (Mix 1) with respect to pool diameter (D) expressed in m and the release rate (v_r), expressed in kPa.

v_r [m s^{-1}]	D [m]				
	0.1	0.5	1.0	2.0	3.0
0.12	$2.59 \cdot 10^{-5}$	$8.06 \cdot 10^{-5}$	$1.44 \cdot 10^{-4}$	$2.74 \cdot 10^{-4}$	$3.89 \cdot 10^{-4}$
10	0.18	0.56	1	1.9	2.7
20	0.72	2.24	4.00	7.60	10.80
40	2.88	8.96	16.00	30.40	43.20

In the table, it is worth noting that ΔP_{max} increases linearly with the diameter for any release rate investigated in this work.

The overpressures calculated by the CFD-LES for all the investigated compositions as a function v_r are reported in Figure 4. The plot is related to a sample distance of 10 m from the source point.
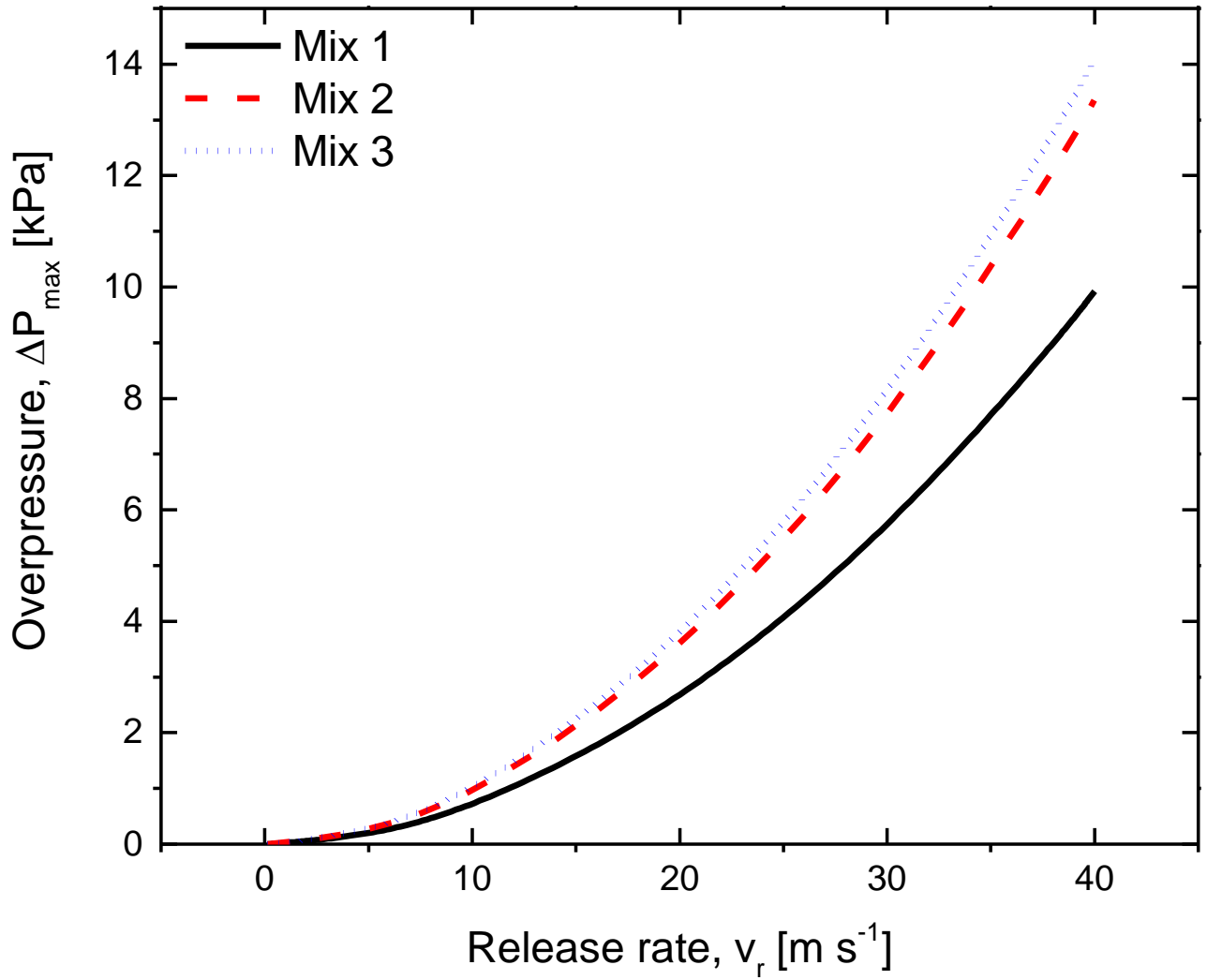
Figure 4. Maximum overpressures generated at 10 m from the releasing point by the accidental release of LNG as a function of the release rate for different mixture compositions. Pool diameter D = 1 m.

Here, it is worth noting that reported estimations of the pressure trends may explain the elevated variability of the data reported by Reid [26], where overpressures within the range 700 – 30000 Pa were reported at 10 m from the releasing point. Besides, a positive parabolic trend for v_r can be identified for all the investigated conditions, thus suggesting that the term related to the kinetic energy of the vapor phase may have a dominant role in the determination of the severity of RPT scenarios. All other diameters analyzed in this work show the same trends with the release rate and the mixture composition.

An empirical-based correlation for the estimation of the maximum overpressure for time ΔP_{max} as a function of release rate v_r and pool diameter (D_p) can then obtained as:

$$\Delta P_{max} = 4 \cdot D_p \cdot \rho_{mix,T_b} \cdot \overline{MW} \cdot v_r^2 \tag{8}$$

where ρ_{mix,T_b} and $\overline{MW}$ are the molar density calculated at the boiling temperature and the average molecular weight of the actual fuel mixture. The accuracy of the given correlation with respect to the numerical predictions obtained in this work is provided in Figure 5.
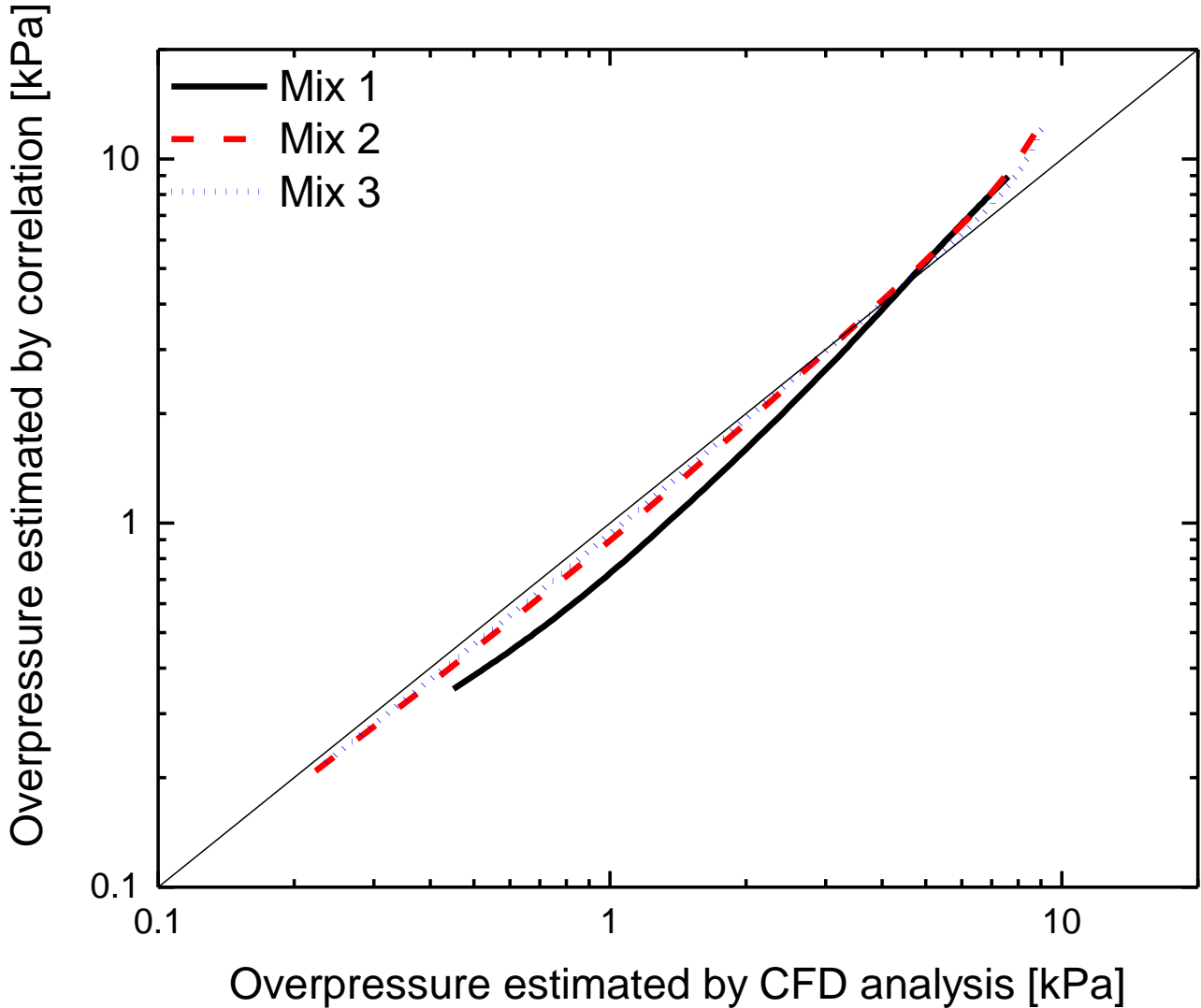

Figure 5. Comparison of the overpressure obtained by means of CFD-LES analysis and simplified correlation (Equation 8), generated by an accidental release of LNG for the release conditions analyzed in this work.

The equation indicates that temperature affects the mixture density, only. Hence, the initial composition of LNG has a limited impact on the temperature representative of the vapor phase layer causing the overpressure, although the boiling temperature variates.

Finally, a limiting velocity (v_{lim}) is essential for the domino effects, taking into consideration the standard value of $\Delta P_{max} = 7\ kPa$, i.e., the lowest value for structural damages [43] [44], for the analyzed compositions (Table 6).

Table 6. Calculated values for the limiting velocity (v_{lim}) giving a maximum overpressure of 7 kPa.

Mixture	v_{lim} [m s^{-1}]
Mix 1	34.11
Mix 2	29.58
Mix 3	28.00

Mix 2 and Mix 3 differences are within 5 % either for maximum overpressure or limiting velocity, whereas both values significantly differ for Mix 1. In particular, the addition of ethane and propane leads to significantly higher overpressure for any investigated release rate, indicating that the assumption of LNG as pure methane does not represent a conservative hypothesis for the RPT scenario. Besides, the reduction of limiting velocity in the case of ethane and propane addition may represent a possible explanation of the correlation between composition and RPT occurrence observed for LNG.

Conclusions

The occurrence of RPT during LNG handling at port facilities or due to the accidental release on the water was found to be relatively unlikely because of the calm water conditions. Indeed, a positive parabolic trend of the maximum overpressure for the release rate was observed, thus demonstrating the dominant role of the kinetic energy. The addition of ethane and propane has a significant effect on generated overpressure, mostly because of the increased molecular weight of the evaporate, as demonstrated by the simplified correlation developed in this work.

References

[1] H. Chen, J. He, and X. Zhong, "Engine combustion and emission fuelled with natural gas : A review," *J. Energy Inst.*, 1–14, 2018.

[2] H. W. Häring and C. Ahner, *Industrial Gases Processing*. 2008.

[3] G. Pio, M. Carboni, T. Iannaccone, V. Cozzani, and E. Salzano, "Numerical simulation of small-scale pool fires of LNG," *J. Loss Prev. Process Ind.*, 61, 82–88, 2019.

[4] O. N. Aneziris, I. A. Papazoglou, M. Konstantinidou, and Z. Nivolianitou, "Integrated risk assessment for LNG terminals," *J. Loss Prev. Process Ind.*, 28, 23–35, 2014.

[5] C. Conrado and V. Vesovic, "The influence of chemical composition on vaporisation of LNG and LPG on unconfined water surfaces," *Chem. Eng. Sci.*, 55, 4549–4562, 2000.

[6] R. Qi, D. Ng, B. R. Cormier, and M. S. Mannan, "Numerical simulations of LNG vapor dispersion in Brayton Fire Training Field tests with ANSYS CFX," *J. Hazard. Mater.*, 183, 51–61, 2010.

[7] G. Pio and E. Salzano, "Laminar Burning Velocity of Methane, Hydrogen and Their Mixtures at Extremely Low Temperature Conditions," *Energy & Fuels*, 32, 8830–8836, 2018.

[8] B. K. Kim, D. Ng, R. A. Mentzer, and M. Sam Mannan, "Key parametric analysis on designing an effective forced mitigation system for LNG spill emergency," *J. Loss Prev.*

Process Ind., 26, 1670–1678, 2013.

[9] G. Pio and E. Salzano, "The effect of ultra-low temperature on the flammability limits of a methane/air/diluent mixtures," *J. Hazard. Mater.*, 362, 224–229, 2019.

[10] E. Aursand and M. Hammer, "Predicting triggering and consequence of delayed LNG RPT," *J. Loss Prev. Process Ind.*, 55, 124–133, 2018.

[11] G. Pio and E. Salzano, "Flammability parameters of liquified natural gas," *J. Loss Prev. Process Ind.*, 56, 424–429, 2018.

[12] R. Bubbico and E. Salzano, "Acoustic analysis of blast waves produced by rapid phase transition of LNG released on water," *Saf. Sci.*, 47, 515–521, 2009.

[13] N. Bariha, V. C. Srivastava, and I. M. Mishra, "Theoretical and experimental studies on hazard analysis of LPG/LNG release: A review," *Rev. Chem. Eng.*, 33, 387–432, 2017.

[14] P. Cleaver, M. Johnson, and B. Ho, "Rapid Phase Transition of LNG," *J. Hazard. Mater.*, 140, 429–438, 2007.

[15] B. Sun, K. Guo, and V. K. Pareek, "Hazardous consequence dynamic simulation of LNG spill on water for ship-to-ship bunkering," *Process Saf. Environ. Prot.*, 107, 402–413, 2017.

[16] M. Gerbec and B. Kontić, "Safety related key performance indicators for securing long-term business development – A case study," *Saf. Sci.*, 98, 77–88, 2017.

[17] J. Zhang, R. Liu, C. Yu, S. Qu, T. Luo, and M. Li, "Numerical simulation of LNG release and dispersion using a multiphase CFD model," *J. Loss Prev. Process Ind.*, 56, 316–327, 2018.

[18] T. L. Morse and H. K. Kytömaa, "The effect of turbulence on the rate of evaporation of LNG on water," *J. Loss Prev. Process Ind.*, 24, 791–797, 2011.

[19] R. G. Scurlock, "The future with cryogenic fluid dynamics," *Phys. Procedia*, 67, 20–26, 2015.

[20] M. Kim, D. Nguyen, and B. Choi, "Experimental study of the evaporation of spreading liquid nitrogen," *J. Loss Prev. Process Ind.*, 39, 68–73, 2016.

[21] F. P. Incropera, D. P. Dewitt, T. L. Bergamm, and A. S. Lavine, *Fundamentals of heat and mass transfer*, 6th ed. John Wiley and Sons, 2007.

[22] N. Gopalaswami, M. S. Mannan, L. Vechot, and T. Olewski, "Small Scale Experimental Study of Vaporization Fluxes of Liquid Nitrogen Released on Water," *29th Cent. Chem. Process Saf. Int. Conf. 2014, CCPS 2014 - Top. Conf. 2014 AIChE Spring Meet. 10th Glob. Congr. Process Saf.*, 433–445, 2014.

[23] O. Basha, T. Olewski, L. Véchot, M. Castier, and S. Mannan, "Modeling of pool spreading of LNG on land," *J. Loss Prev. Process Ind.*, 30, 307–314, 2014.

[24] J. L. Woodward and R. M. Pitblado, "LNG RISK BASED SAFETY Modeling and Consequence Analysis."

[25] E. K. Kalinin, I. I. Berlin, V. V. Kostyuk, and E. M. Nosova, "Heat Transfer in Transition Boiling of Cryogenic Liquids," in *Advances in Cryogenic Engineering*, 1960.

[26] R. C. Reid, *Rapid phase transitions from liquid to vapor*, 12. 1983.

[27] V. V. Klimenko, "Film boiling on a horizontal plate - new correlation," *Int. J. Heat Mass Transf.*, 24, 69–79, 1981.

[28] A. Luketa-Hanlin, "A review of large-scale LNG spills: Experiments and modeling," *J. Hazard. Mater.*, 132, 119–140, 2006.

[29] A. Luketa-Hanlin, E. Scientific, P. Company, C. Brons, C. Olieman, A. Parihar, C. Vergara, J. K. Clutter, O. Aneziris, I. Koromila, and Z. Nivolianitou, "Methodology for consequence analysis of LNG releases at deepwater port facilities," *Saf. Sci.*, 124, 104595, 2011.

[30] G. F. Feldbauer, J. J. Heigl, W. McQueen, R. H. Whipp, and W. G. May, "Spills of LNG on water — vaporization and downwind drift of combustible mixtures, API Report EE61E-72," 1972.

[31] D. A. McQuarrie and J. D. Simon, *Physical chemistry - A molecular Approach*. 2008.

[32] D. Nédelka, V. Sauter, J. Goanvic, and R. Ohba, "Last developments in Rapid Phase Transition knowledge and modeling techniques," *Offshore Technol. Conf.*, 2003.

[33] C. J. Greenshields, "OpenFOAM," 2015.

[34] G. Pio, M. Carboni, and E. Salzano, "Realistic aviation fuel chemistry in computational fluid dynamics," *Fuel*, 254, 2019.

[35] A. Luketa-Hanlin, R. P. Koopman, and D. L. Ermak, "On the application of computational fluid dynamics codes for liquefied natural gas dispersion," *J. Hazard. Mater.*, 140, 504–517, 2007.

[36] K. Verfondern, "Experimental and Theoretical Investigation of Liquid Hydrogen Pool Spreading and Vaporization," *Int. J. Hydrogen Energy*, 22, 649–660, 1997.

[37] O. Aneziris, I. Koromila, and Z. Nivolianitou, "A systematic literature review on LNG safety at ports," *Saf. Sci.*, 124, 104595, 2020.

[38] Niigata Loading System LTD, "Marine Loading Arms," 2019.

[39] British Standards Institution, "BSI Standards Publication Natural gas — Quality designation (ISO 13686 : 2013)," 2013.

[40] F. C. Pickard, E. K. Pokon, M. D. Liptak, and G. C. Shields, "Comparison of CBS-QB3, CBS-APNO, G2, and G3 thermochemical predictions with experiment for formation of ionic clusters of hydronium and hydroxide ions complexed with water," *J. Chem. Phys.*, 122, 1–7, 2005.

[41] "Arkane - https://github.com/ReactionMechanismGenerator/RMG-Py/tree/master/arkane," 2020. .

[42] A. Grinberg Dana, D. Ranasinghe, H. Wu, C. Grambow, X. Dong, M. Johnson, M. Goldman, M. Liu, and W. H. Green, "'ARC - Automated Rate Calculator', version 1.1.0," *DOI: 10.5281/zenodo.3356849.* .

[43] G. Atkinson, L. Cusco, D. Painter, and V. Tam, "Interpretation of overpressure markers and directional indicators in full-scale deflagrations and detonations," *Inst. Chem. Eng. Symp. Ser.*, 500–506, 2009.

[44] V. Cozzani and E. Salzano, "Threshold values for domino effects caused by blast wave interaction with process equipment," *J. Loss Prev. Process Ind.*, 17, 437–447, 2004.